Abiotic production of sugar phosphates and uridine ribonucleoside in aqueous microdroplets

Inho Nam[a,b], Jae Kyoo Lee[a], Hong Gil Nam[b,c,1], and Richard N. Zare[a,1]

[a]Department of Chemistry, Stanford University, Stanford, CA 94305; [b]Center for Plant Aging Research, Institute for Basic Science, Daegu 42988, Republic of Korea; and [c]Department of New Biology, Daegu Gyeongbuk Institute of Science and Technology (DGIST), Daegu 42988, Republic of Korea

Contributed by Richard N. Zare, September 21, 2017 (sent for review August 23, 2017; reviewed by R. Graham Cooks and Veronica Vaida)

Phosphorylation is an essential chemical reaction for life. This reaction generates fundamental cell components, including building blocks for RNA and DNA, phospholipids for cell walls, and adenosine triphosphate (ATP) for energy storage. However, phosphorylation reactions are thermodynamically unfavorable in solution. Consequently, a long-standing question in prebiotic chemistry is how abiotic phosphorylation occurs in biological compounds. We find that the phosphorylation of various sugars to form sugar-1-phosphates can proceed spontaneously in aqueous microdroplets containing a simple mixture of sugars and phosphoric acid. The yield for D-ribose-1-phosphate reached over 6% at room temperature, giving a ΔG value of −1.1 kcal/mol, much lower than the +5.4 kcal/mol for the reaction in bulk solution. The temperature dependence of the product yield for the phosphorylation in microdroplets revealed a negative enthalpy change (ΔH = −0.9 kcal/mol) and a negligible change of entropy (ΔS = 0.0007 kcal/mol·K). Thus, the spontaneous phosphorylation reaction in microdroplets occurred by overcoming the entropic hurdle of the reaction encountered in bulk solution. Moreover, uridine, a pyrimidine ribonucleoside, is generated in aqueous microdroplets containing D-ribose, phosphoric acid, and uracil, which suggests the possibility that microdroplets could serve as a prebiotic synthetic pathway for ribonucleosides.

sugar phosphorylation | uracil ribosylation | microdroplet chemistry | prebiotic chemistry | origin of life

Phosphorylation is an essential reaction in all cells and is involved in most processes, including metabolism, DNA replication, and signaling (1). Phosphorylation changes the biochemical and structural properties of various target molecules, activates molecules for subsequent reactions, and is used to store and retrieve biological energy (2–4). For instance, the phosphorylation of glucose is an important step in glycolysis, the fundamental metabolic pathway in any cell (4), and the phosphorylation of ribose is required to form building blocks for ribonucleosides (5–7). In a biotic environment, the synthesis of the ribonucleosides takes a salvage pathway in which ribose-1-phosphate and nucleobases are changed to ribonucleosides and phosphate (6, 7). Given that phosphorylation is required for life, identifying plausible routes for phosphorylation reactions in prebiotic conditions has been a long-standing challenge (1, 8, 9).

However, phosphorylation reactions involve an increased Gibbs free-energy change (ΔG) and are thus unfavorable in bulk solution. For example, the Gibbs free-energy changes for abiotic phosphorylation of D-ribose and D-glucose in bulk solution are ΔG = +5.4 kcal/mol (10) and +3.3 kcal/mol (11), respectively. For the reaction between uracil and ribose-1-phosphate, ΔG = –0.73 kcal/mol (12); therefore, once ribose-1-phosphate is formed, the reaction to make uridine occurs spontaneously. These phosphorylation reactions are also highly unfavorable in water owing to the thermodynamic instability of phosphate compounds with respect to hydrolysis (the "water problem" in prebiotic chemistry) (13–15). Moreover, even if we can resolve the thermodynamic problems, the kinetics would be another obstacle for these reactions. Cells utilize kinase enzymes and ATPs to overcome these thermodynamic and kinetic hurdles (11). Consequently, a plausible route of phosphorylation reaction under prebiotic conditions has yet to be established. In the same manner, the abiotic ribosylation of pyrimidine nucleobases also suffers from the same set of problems (16).

Microdroplets exhibit chemical reaction properties that are not observed in bulk solution. Recent studies have shown some reactions can be accelerated in microdroplets compared with bulk solution. We and other groups already have shown that the reaction rates for various chemical and biochemical reactions, including redox reactions (17, 18), protein unfolding (19), chlorophyll demetallation (20), addition/condensation reactions (21), carbon–carbon bond-forming reactions (22), and elimination/substitution reactions (23) are accelerated by 10^3 to 10^6-fold in microdroplets compared with bulk solution. Based on these studies, we hypothesized that microdroplets would affect the kinetic and thermodynamic properties of phosphorylation reactions.

It has been suggested that the air–water or vesicle interface may provide a favorable environment for the prebiotic synthesis of biomolecules (24–28). For example, there is an earlier study on the reaction between serine and other compounds of fundamental importance in prebiotic chemistry, including glyceraldehyde, glucose, and phosphoric acid in sonic-sprayed microdroplets (29). From this background, here we investigated the use of microdroplets to effect phosphorylation of sugars and the formation of uridine.

Results

We performed phosphorylation reactions (see Fig. S1 for reaction scheme) in aqueous microdroplets containing sugars and

Significance

Phosphorylation is essential for life. Phosphorylated molecules play diverse functions in cells, including metabolic (e.g., sugar phosphates), structural (e.g., phospholipids), and instructional (e.g., RNA and DNA). In nature, the phosphorylation of sugars via condensation is thermodynamically and kinetically unfavorable in bulk solution. Thus, a key question arising within prebiotic chemistry concerning the origin of life is, "How was phosphorus incorporated into the biological world?" Here, we show that sugar phosphates and a ribonucleoside form spontaneously in microdroplets, without enzymes or an external energy source. Sugar phosphorylation in microdroplets has a lower entropic cost than in bulk solution. Therefore, thermodynamic obstacles of prebiotic condensation reactions can be circumvented in microdroplets.

Author contributions: I.N., J.K.L, H.G.N., and R.N.Z. designed the projects; I.N. conducted experiments and analyzed data; I.N., J.K.L, H.G.N., and R.N.Z. interpreted and discussed the data; H.G.N. and R.N.Z. directed and supervised the project; and I.N., J.K.L, H.G.N., and R.N.Z. wrote the manuscript.

Reviewers: R.G.C., Purdue University; and V.V., University of Colorado.

The authors declare no conflict of interest.

See Commentary on page 12359.

[1]To whom correspondence may be addressed. Email: nam@dgist.ac.kr or zare@stanford.edu.

This article contains supporting information online at www.pnas.org/lookup/suppl/doi:10.1073/pnas.1714896114/-/DCSupplemental.

phosphoric acid. Microdroplets were generated (Fig. 1*A*) by atomization of a bulk solution containing a mixture of 5 mM sugar (D-ribose, L-ribose, D-glucose, D-galactose, or D-fructose) and 5 mM phosphoric acid with a nebulizing gas (dry N_2) at 120 psi, using an electrospray ionization (ESI) source placed in front of a high-resolution mass spectrometer (MS) (17). Under these conditions, the sizes of droplets were reported to range from 1 to 50 μm (30–32). The droplets were positively charged by external application of a potential of 5 kV to the ESI source to facilitate Coulomb droplet fission and the ionization of molecular species. The microdroplets traveled 25 mm at room temperature and atmospheric pressure before the reaction was stopped upon entering the MS inlet (19). The approximate flight time and corresponding reaction time were estimated to be ~300 μs on the basis of the droplet speed (~80 m/s) (30, 33).

In each mass spectrum, we observed new peaks that were not present in the reactant solution (Fig. 1 *B–E* and Fig. S2). In particular, peaks at m/z = 231.026 for ribose and m/z = 261.038 for glucose, galactose, and fructose (Fig. 1 *B–E*) were identified as ribose-phosphate $[\text{Rib-P} + H^+]^+$, glucose-phosphate $[\text{Glu-P} + H^+]^+$, galactose-phosphate $[\text{Gal-P} + H^+]^+$, and fructose-phosphate $[\text{Fru-P} + H^+]^+$. Thus, sugar phosphorylation proceeds spontaneously at room temperature and atmospheric pressure in aqueous microdroplets containing sugar and phosphoric acid, without any enzyme or ATP.

For a quantitative analysis, we measured the ionization efficiencies of sugar phosphates and phosphoric acid and generated calibration curves for each analyte (Fig. S3). We then converted the ratio of the peak intensity between the sugar phosphate and phosphoric acid into the concentration ratio. We calculated the product yield for phosphorylation of ribose, glucose, galactose, and fructose in 300 μs was ~6%, 13%, 13%, and 10%, respectively, in charged microdroplets.

Each sugar could theoretically have multiple phosphorylated forms, depending on the position and number of phosphate groups bound to the sugar. Here, we observed only monophosphorylated sugar species. In nature, ribose monophosphate exists as ribose-1-phosphate and ribose-5-phosphate (5). The monophosphates of glucose, galactose, and fructose exist as sugar-1-phosphate and sugar-6-phosphate (34). To determine the isomeric form of the sugar monophosphates generated in the microdroplets, we performed tandem mass spectrometry using collision-induced dissociation (CID). The fragmentation pattern of the sugar monophosphates from each microdroplet reaction matched that of the respective sugar-1-phosphates (Fig. S4). Thus, the phosphorylation of the sugars by phosphoric acid in microdroplets specifically favors the hydroxyl residue at the C1 positions of the sugars.

As the mass spectrometry cannot distinguish between the two optical isomers, D- and L-sugars, we tested if there was any

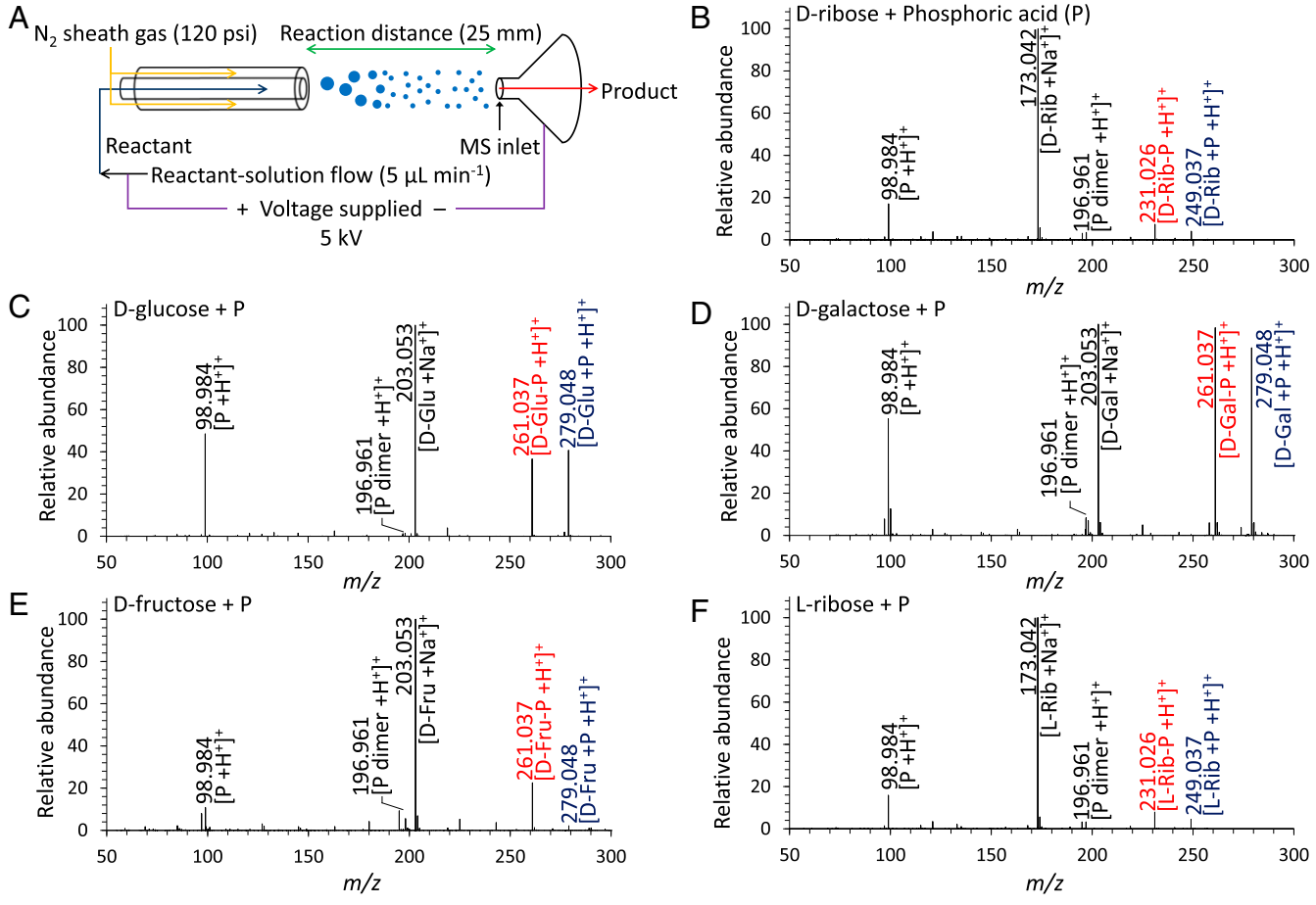

Fig. 1. Mass spectra of the sugar phosphates produced from microdroplet reactions. (*A*) Schematic diagram showing synthesis of the sugar phosphates produced from the reaction between sugars and phosphoric acid in microdroplets, recorded by a high-resolution MS. (*B–F*) Mass spectra of the products from each sugar phosphorylation reaction. The red numbers and letters denote the detected m/z peaks of phosphorylated sugars, identified as (*B*) D-ribose-phosphate (D-Rib-P), (*C*) D-glucose-phosphate (D-Glu-P), (*D*) D-galactose-phosphate (D-Gal-P), (*E*) D-fructose-phosphate (D-Fru-P), and (*F*) L-ribose-phosphate (L-Rib-P). The blue numbers and letters denote the aggregated species between each sugar and phosphate. The black numbers and letters denote the species present within the reactants.

transformation of the optical isomeric forms during the phosphorylation in microdroplets. The specific rotations, $[\alpha]_D^{20}$, of D-ribose and D-ribose-1-phosphate are −25.0° and +39.8°, respectively (35, 36). The $[\alpha]_D^{20}$ of the solution collected from the reaction between D-ribose and ribose-1-phosphate in microdroplets was measured to be −21.1° by a polarimeter. This value indicates that a small amount (~6%) of D-ribose-1-phosphate is generated from D-ribose and phosphoric acid. Thus, ribose-1-phosphate maintains the same chirality as the starting ribose after the reaction in the microdroplets.

Next, we tested whether the external voltage applied to the microdroplets may have driven the unfavorable condensation reaction between phosphoric acid and D-ribose. Even without applying an external charge, D-ribose was spontaneously phosphorylated to D-ribose-1-phosphate in microdroplets, although the signal intensity of D-ribose-1-phosphate relative to the reactant's signal intensity was somewhat lower than that observed with an external charge (Fig. S5*A*). Phosphorylation of the other sugars also did not require an external charge (Fig. S5 *B* and *C*). The product yields for the phosphorylation of ribose, glucose, galactose, and fructose were ~3%, 11%, 11%, and 7%, respectively, in uncharged microdroplets. These yields are comparable to that of phosphorylation reaction in bulk solution conducted from 3 h to 1 d using cyanogen as a condensing agent and an orthophosphate ion (PO_4^{3-}) (37, 38). In conclusion, an external charge, condensing matter, and organic phosphates as an energy source are not required for phosphorylation of sugars in aqueous microdroplets.

To determine the time required for the reaction to reach equilibrium, we measured the ratio of the peak intensity between D-ribose-1-phosphate and unreacted D-ribose at various reaction times in charged and uncharged microdroplets (Fig. 2). To vary the reaction time, we changed the distance traveled by microdroplets from the sprayer source tip to the inlet of the MS. The evaporation of microdroplet solvents can change droplet size and hence the reaction rates (21). However, aqueous microdroplets show negligible evaporation during their flight time, from tens to hundreds of microseconds (19, 39). Therefore, the size and the temperature of the microdroplets are predicted to be essentially unchanged during the time of observation in the present studies. We found that the reaction had progressed substantially on the order of tens of microseconds and reached equilibrium in ~200 μs, irrespective of charge. The forward reaction constant of the ribose phosphorylation in uncharged microdroplets was 280/mM·s.

We examined the thermodynamic properties of the phosphorylation of D-ribose in microdroplets. The reported value (+5.4 kcal/mol) of ΔG for the reaction in bulk solution (10) indicates the reaction would not proceed in bulk solution spontaneously. However, in microdroplets, the reaction proceeded spontaneously, producing a significant amount of D-ribose-1-phosphate. Thus, ribose phosphorylation by phosphoric acid in microdroplets should have a different thermodynamic property than the reaction in bulk solution, and should have a lower ΔG value. To determine the free-energy change for ribose phosphorylation in microdroplets, we used the equation $\Delta G = -RT \ln K$, which relates to equilibrium constant K, where R is the universal gas constant. As the ribose phosphorylation reaction reached equilibrium within our experiment, we were able to derive ΔG from the equilibrium concentration. The ΔG value for D-ribose phosphorylation was −1.1 kcal/mol at room temperature, in sharp contrast to the reported value of +5.4 kcal/mol for bulk solution (10).

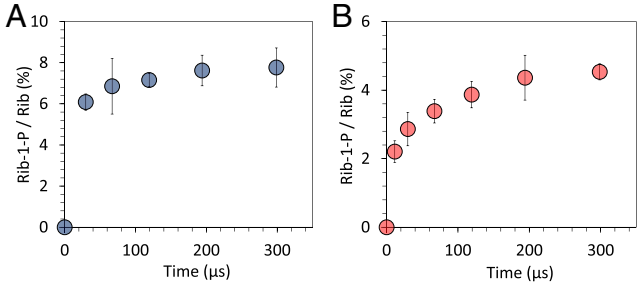

Fig. 2. Progression of the phosphorylation reaction between D-ribose and phosphoric acid in charged and uncharged aqueous microdroplets. Time-course changes in the ion count ratio between D-ribose-1-phosphate and unreacted D-ribose in (*A*) charged and (*B*) uncharged microdroplets. Error bars represent 1 SD from triple measurements.

Table 1. Values of the equilibrium constant (K) and the change in Gibbs free energy (ΔG) for phosphorylation of D-ribose-1-phosphate in uncharged microdroplets at various temperatures

Temperature, K	K	ΔG, kcal/mol
273	8.3	−1.1
298	6.9	−1.1
353	5.5	−1.2

This is in agreement with a free-energy decrease observed in emulsion droplets for the imime synthesis reaction that led to reaction acceleration (25). However, the ΔG for the reaction in emulsion droplets remained still in a positive value, unlike our studies. Our results show that an unfavorable reaction with a positive ΔG in bulk solution can become a reaction with a negative ΔG in microdroplets, which suggest that it may be possible to cause even thermodynamically unfavorable reactions to happen in microdroplets.

To further understand the thermodynamic behavior of ribose phosphorylation in microdroplets, we determined how temperature variation affects the yield of the D-ribose-1-phosphate production (Table 1). We found that there is little change in the ΔG value between 237 to 317 K (−1.1 kcal/mol), implying that the entropy change in the phosphorylation is negligible in microdroplets. By using the equations $\Delta G = \Delta H - T\Delta S$, we derived $\Delta H = -0.9$ kcal/mol, and $\Delta S = 7 \times 10^{-4}$ kcal/mol·K from the Van 't Hoff plot (Fig. 3). The $T\Delta S$ value (0.2 kcal/mol at room temperature) is much smaller than the ΔH value, which means that ribose phosphorylation in microdroplets is driven mostly by a change in enthalpy. This phosphorylation reaction is entropically unfavorable in bulk solution (1, 40). Therefore, we conclude that the entropic obstacle is overcome in the microdroplet environment, which may involve surface and near-surface reactions (41). Interestingly, the observed ΔH value in microdroplets is very close to the value ($\Delta H = -1.02$ kcal/mol) calculated from a density-functional theory (DFT) based on the projector-augmented wave method for the reaction involving unsolvated reactants and products (Fig. S6 and Table S1).

To show the abiotic synthesis of a pyrimidine ribonucleoside, we performed ribosylation reaction in aqueous microdroplets containing D-ribose, phosphoric acid, and uracil. As shown in Fig. 4, we observed new peaks that were not present in the phosphorylation reaction between D-ribose and phosphate. In particular, peaks at $m/z = 245.077$ and $m/z = 263.088$ were identified as uridine $[\text{uridine} + H^+]^+$ and an aggregate between ribose and uracil $[\text{D-Rib} + \text{uracil} + H^+]^+$. Thus, uridine also forms spontaneously at room temperature and atmospheric pressure in aqueous microdroplets. In the microdroplets containing only D-ribose and uracil without phosphoric acid, ribosylation reaction products were not observed. These results indicate that this reaction may follow a similar route to a salvage pathway in cells (6, 7). From calibration of ionization efficiency between uridine and uracil, the yield of uridine production is ~2.5% in charged microdroplets under our conditions.

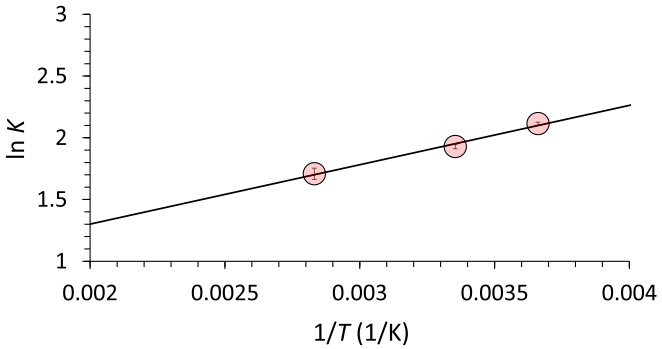

Fig. 3. Van 't Hoff plot for phosphorylation of D-ribose-1-phosphate in uncharged microdroplets. ΔH and ΔS are calculated as $\Delta H = -0.9$ kcal/mol and $\Delta S = 0.7$ cal/mol·K. Error bars represent one SD from triple measurements. The slope of this plot yields $-\Delta H/R$ and the intercept $\Delta S/R$.

Discussion

Aqueous microdroplets are abundant in nature. Obvious examples include clouds and aerosols in the atmosphere, as well as microdroplets produced by breaking waves in the ocean and water sprays. We showed the abiotic and nonenzymatic synthesis of various sugar phosphates and one ribonucleoside (uridine) in micrometer-sized aqueous droplets under ambient conditions of 1 atmosphere and room temperature. We found that sugar phosphorylation in microdroplets had a reduced entropic cost compared with the reaction in bulk solution. As a result, ΔG for the reaction in microdroplets is negative and the reaction is favorable, in sharp contrast to the reaction in bulk solution. Aqueous microdroplets possess properties that can promote chemical reactions including catalysis, molecular organization, facilitated diffusion, and electric field at the air–water interface. The decreased entropic change for chemical reactions in microdroplets could be attributed to the molecular organization and alignment of reactants at the air–water interface of microdroplet surfaces (42–49). The air–water interface possesses a strong electric field, which could influence the organization of reactant molecules, as well as the kinetics and thermodynamics of chemical reactions (50). We speculate that these surface properties contribute to the spontaneous phosphorylation reactions we observed.

We thus propose that aqueous microdroplets might be a highly plausible means for forming biologically available phosphorus-containing compounds. Our findings might have important implications for how biologically relevant molecules were generated in the prebiotic era (25, 28, 51).

Methods

Experimental Design for the Generation of Microdroplets. The aqueous solution of sugar and phosphoric acid was injected by a mechanical syringe pump through a hypodermic needle to the fused silica capillary directing toward an MS inlet. A coaxial sheath gas (dry N_2 at 120 psi) flow around the capillary results in nebulization, and also helps to direct the spray emerging from the capillary tip toward the MS inlet (the flow rate of 5 μL/min through silica tubing). Two different voltages of 0 and +5 kV were applied to the hypodermic needle. At an MS inlet, the reactants, intermediates, and products are released from droplets by Coulomb fission and enter into the MS through a heated capillary. The capillary temperature was maintained at 275 °C and capillary voltage at 44 V. To confirm the identities of synthesized phosphorylated sugars, tandem mass spectrometry was conducted by CID. The spray distance (the distance from spray tip to the entrance of the heated capillary) was varied from 2 to 25 mm for monitoring the progression of reaction. For all other mass spectrometric analyses, the spray distance was kept at 25 mm. Mass spectra were detected by a high-resolution MS (LTQ Orbitrap XL Hybrid Ion Trap-Orbitrap; Thermo Scientific). All of the necessary chemicals were purchased from Sigma-Aldrich. HPLC-grade solvents were purchased from Fisher Scientific.

Quantitative Analysis. The quantitative analysis for the estimate of percentage yield of the above reactions was performed by the standard calibration

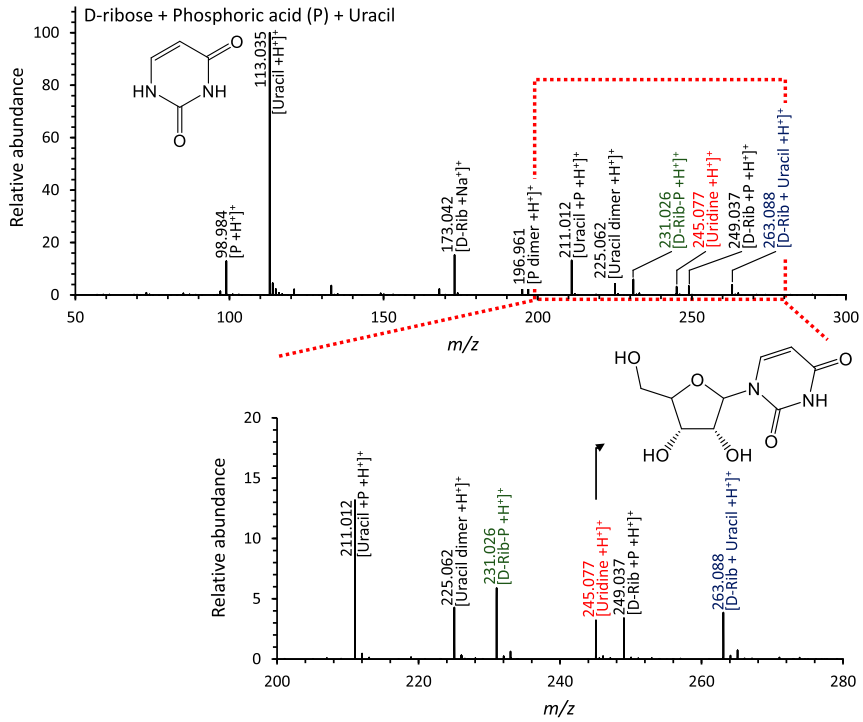

Fig. 4. Mass spectra of the products from ribosylation reaction of uracil with ribose and phosphoric acid in microdroplets. The *m/z* peak of protonated uridine is in red, the protonated complex of D-ribose with uracil is in blue, and the protonated ribose-phosphate intermediate is in green. The black numbers and letters denote species in the reactants.

method. Standard calibration plots were made from electric spraying the mixture of the reactant (phosphoric acid) and the corresponding authentic product (sugar phosphate) in known concentration ratios. The initial mixture contained phosphoric acid at a concentration of 5 mM and the standard product of concentration 0 mM. Then the product concentration was increased gradually. As the ion signal intensities of the reactant (I_R) and the product (I_P) depend both on their concentrations and ionization efficiencies, we calculated the ratio I_P/I_R (averaged over time) and plotted it against the product-to-reactant concentration ratio ([P]/[R]). We have estimated the yield of the reaction from this standard calibration plot.

Solution temperature was varied from 273 to 353 K for calculation of the change in enthalpy, ΔH, and entropy, ΔS, of the phosphorylation of sugar in uncharged microdroplets using $\Delta G = \Delta H - T\Delta S$. In this calibration, it is possible that the solution temperature before nebulization was slightly different from a droplet temperature, but the difference of temperature is negligible in 100 μs (52, 53).

DFT Calculations. First-principles calculations were carried out on the basis of periodic DFT using a generalized gradient approximation within the Perdew–Burke–Ernzerhof exchange correlation functional (54, 55). We used the projector-augmented wave method for describing ionic cores as implemented in the Vienna ab initio simulation package (VASP) (56). The wave functions were constructed from the expansion of plane waves with an energy cutoff of 520 eV. A $6 \times 6 \times 6$ k-point mesh described in Monkhorst–Pack method was used to sample the Brillouin zone. The electronic optimization steps were converged self-consistently over 10^{-4} eV per formula unit.

ACKNOWLEDGMENTS. The authors thank Life Science Editors for editorial assistance. This work was supported by the Institute for Basic Science (IBS-R013-D1) and the Air Force Office of Scientific Research through the Basic Research Initiative Grant (AFOSR FA9550-12-1-0400). We dedicate this paper to the memory of Alexandra Hyunji Nam (1987–2017).

1. Gull M (2014) Prebiotic phosphorylation reactions on the early earth. *Challenges* 5: 193–212.
2. Manning G, Whyte DB, Martinez R, Hunter T, Sudarsanam S (2002) The protein kinase complement of the human genome. *Science* 298:1912–1934.
3. Westheimer FH (1987) Why nature chose phosphates. *Science* 235:1173–1178.
4. Saier MH, Jr (1989) Protein phosphorylation and allosteric control of inducer exclusion and catabolite repression by the bacterial phosphoenolpyruvate: Sugar phosphotransferase system. *Microbiol Rev* 53:109–120.
5. Tozzi MG, Camici M, Mascia L, Sgarrella F, Ipata PL (2006) Pentose phosphates in nucleoside interconversion and catabolism. *FEBS J* 273:1089–1101.
6. Mascia L, Cappiello M, Cherri S, Ipata PL (2000) In vitro recycling of alpha-D-ribose 1-phosphate for the salvage of purine bases. *Biochim Biophys Acta* 1474:70–74.
7. Cappiello M, Mascia L, Scolozzi C, Giorgelli F, Ipata PL (1998) In vitro assessment of salvage pathways for pyrimidine bases in rat liver and brain. *Biochim Biophys Acta* 1425:273–281.
8. Thaxton C, Bradley W, Olsen R (1984) *The Mystery of Life's Origin: Reassessing Current Theories* (Philosophical Library, New York).
9. Cairns-Smith A (1982) *Genetic Takeover: And the Mineral Origin of Life* (Cambridge Univ Press, New York).
10. Camici M, Sgarrella F, Ipata PL, Mura U (1980) The standard Gibbs free energy change of hydrolysis of alpha-D-ribose 1-phosphate. *Arch Biochem Biophys* 205:191–197.
11. Lodish H, et al. (2000) *Molecular Cell Biology* (W. H. Freeman, New York).
12. Latendresse M (2013) Computing Gibb's free energy of compounds and reactions in MetaCyc. Available at https://biocyc.org/META/NEW-IMAGE?type=REACTION&object=URPHOS-RXN. Accessed September 6, 2017.
13. Furukawa Y, Kim H-J, Hutter D, Benner SA (2015) Abiotic regioselective phosphorylation of adenosine with borate in formamide. *Astrobiology* 15:259–267.
14. Neveu M, Kim H-J, Benner SA (2013) The "strong" RNA world hypothesis: Fifty years old. *Astrobiology* 13:391–403.
15. Benner SA, Kim H-J, Carrigan MA (2012) Asphalt, water, and the prebiotic synthesis of ribose, ribonucleosides, and RNA. *Acc Chem Res* 45:2025–2034.
16. Powner MW, Gerland B, Sutherland JD (2009) Synthesis of activated pyrimidine ribonucleotides in prebiotically plausible conditions. *Nature* 459:239–242.
17. Lee JK, Banerjee S, Nam HG, Zare RN (2015) Acceleration of reaction in charged microdroplets. *Q Rev Biophys* 48:437–444.
18. Banerjee S, Zare RN (2015) Syntheses of isoquinoline and substituted quinolines in charged microdroplets. *Angew Chem Int Ed Engl* 54:14795–14799.
19. Lee JK, Kim S, Nam HG, Zare RN (2015) Microdroplet fusion mass spectrometry for fast reaction kinetics. *Proc Natl Acad Sci USA* 112:3898–3903.
20. Lee JK, Nam HG, Zare RN (2017) Microdroplet fusion mass spectrometry: Accelerated kinetics of acid-induced chlorophyll demetallation. *Q Rev Biophys* 50:1–7.
21. Girod M, Moyano E, Campbell DI, Cooks RG (2011) Accelerated bimolecular reactions in microdroplets studied by desorption electrospray ionization mass spectrometry. *Chem Sci* 2:501–510.
22. Müller T, Badu-Tawiah A, Cooks RG, Graham R (2012) Accelerated carbon-carbon bond-forming reactions in preparative electrospray. *Angew Chem Int Ed Engl* 51:11832–11835.
23. Yan X, Bain RM, Cooks RG (2016) Organic reactions in microdroplets: Reaction acceleration revealed by mass spectrometry. *Angew Chem Int Ed Engl* 55:12960–12972.
24. Walde P, Umakoshi H, Stano P, Mavelli F (2014) Emergent properties arising from the assembly of amphiphiles. Artificial vesicle membranes as reaction promoters and regulators. *Chem Commun (Camb)* 50:10177–10197.
25. Fallah-Araghi A, et al. (2014) Enhanced chemical synthesis at soft interfaces: A universal reaction-adsorption mechanism in microcompartments. *Phys Rev Lett* 112: 028301.
26. Griffith EC, Vaida V (2012) In situ observation of peptide bond formation at the water-air interface. *Proc Natl Acad Sci USA* 109:15697–15701.
27. Tuck A (2002) The role of atmospheric aerosols in the origin of life. *Surv Geophys* 23: 379–409.
28. Dobson CM, Ellison GB, Tuck AF, Vaida V (2000) Atmospheric aerosols as prebiotic chemical reactors. *Proc Natl Acad Sci USA* 97:11864–11868.
29. Takats Z, Nanita SC, Cooks RG (2003) Serine octamer reactions: Indicators of prebiotic relevance. *Angew Chem Int Ed Engl* 42:3521–3523.
30. Venter A, Sojka PE, Cooks RG (2006) Droplet dynamics and ionization mechanisms in desorption electrospray ionization mass spectrometry. *Anal Chem* 78:8549–8555.
31. Smith JN, Flagan RC, Beauchamp JL (2002) Droplet evaporation and discharge dynamics in electrospray ionization. *J Phys Chem A* 106:9957–9967.
32. Ganan-Calvo AM, Davila J, Barrero A (1997) Current and droplet size in the electrospraying of liquids scaling laws. *J Aerosol Sci* 28:249–275.
33. Wang R, et al. (2011) The role of nebulizer gas flow in electrosonic spray ionization (ESSI). *J Am Soc Mass Spectrom* 22:1234–1241.
34. Meyerhof O, Green H (1949) Synthetic action of phosphatase; equilibria of biological esters. *J Biol Chem* 178:655–667.
35. Kline P (2017) Identification of an unknown saccharide. Available at homepage.smc.edu/kline_peggy/Organic/Lab_Reports_Ch_24/Sugar_Unknown_New.pdf. Accessed September 6, 2017.
36. Bunton CA, Humeres E (1969) The hydrolyses of alpha-D-ribose and alpha-D-glucose 1-phosphate. *J Org Chem* 34:572–576.
37. Degani Ch, Halmann M (1971) D-glucose 1-phosphate formation by cyanogen-induced phosphorylation of D-glucose. Synthesis, mechanism, and application to other reducing sugars. *J Chem Soc C* 0:1459–1465.
38. Halmann M, Sanchez RA, Orgel LE (1969) Phosphorylation of D-ribose in aqueous solution. *J Org Chem* 34:3702–3703.
39. Jansson ET, Lai Y-H, Santiago JG, Zare RN (2017) Rapid hydrogen-deuterium exchange in liquid droplets. *J Am Chem Soc* 139:6851–6854.
40. Page MI, Jencks WP (1971) Entropic contributions to rate accelerations in enzymic and intramolecular reactions and the chelate effect. *Proc Natl Acad Sci USA* 68:1678–1683.
41. Banerjee S, Gnanamani E, Yan X, Zare RN (2017) Can all bulk-phase reactions be accelerated in microdroplets? *Analyst (Lond)* 142:1399–1402.
42. Chen X, Minofar B, Jungwirth P, Allen HC (2010) Interfacial molecular organization at aqueous solution surfaces of atmospherically relevant dimethyl sulfoxide and methanesulfonic acid using sum frequency spectroscopy and molecular dynamics simulation. *J Phys Chem B* 114:15546–15553.
43. Matsuzawa Y, Yokokawa S, Ichimura K (2002) Molecular organization of aminimides with long-alkyl chains on water surface. *Colloids Surf A Physicochem Eng Asp* 198: 165–172.
44. Gassin P-M, et al. (2015) Surface activity and molecular organization of metallacarboranes at the air-water interface revealed by nonlinear optics. *Langmuir* 31: 2297–2303.
45. Shultz MJ, Vu TH, Meyer B, Bisson P (2012) Water: A responsive small molecule. *Acc Chem Res* 45:15–22.
46. Donaldson DJ, Vaida V (2006) The influence of organic films at the air-aqueous boundary on atmospheric processes. *Chem Rev* 106:1445–1461.
47. Tervahattu H, et al. (2005) Fatty acids on continental sulfate aerosol particles. *J Geophys Res* 110:D06207.
48. Tervahattu H, Juhanoja J, Kupiainen K (2002) Identification of an organic coating on marine aerosol particles by TOF-SIMS. *J Geophys Res Atmos* 107:ACH 18-1–ACH 18-7.
49. Watry MR, Richmond GL (2002) Orientation and conformation of amino acids in monolayers adsorbed at an oil/water interface as determined by vibrational sum-frequency spectroscopy. *J Phys Chem B* 106:12517–12523.
50. Kathmann SM, Kuo I-FW, Mundy CJ (2008) Electronic effects on the surface potential at the vapor-liquid interface of water. *J Am Chem Soc* 130:16556–16561.
51. Hallquist M, et al. (2009) The formation, properties and impact of secondary organic aerosol: Current and emerging issues. *Atmos Chem Phys* 9:5155–5236.
52. Wang C, Xu R, Song Y, Jiang R (2017) Study on water droplet flash evaporation in vacuum spray cooling. *Int J Heat Mass Transfer* 112:279–288.
53. Kincaid DC, Longley TS (1989) A water droplet evaporation and temperature model. *Trans ASAE* 32:457–462.
54. Kresse G, Furthmüller J (1996) Efficient iterative schemes for ab initio total-energy calculations using a plane-wave basis set. *Phys Rev B Condens Matter* 54:11169–11186.
55. Perdew JP, Burke K, Ernzerhof M (1996) Generalized gradient approximation made simple. *Phys Rev Lett* 77:3865–3868.
56. Blöchl PE (1994) Projector augmented-wave method. *Phys Rev B Condens Matter* 50: 17953–17979.